PNAS RESEARCH ARTICLE | SYSTEMS BIOLOGY OPEN ACCESS

Evaluating plant growth–defense trade-offs by modeling the interaction between primary and secondary metabolism

Jan Zrimec[a,1,2], Sandra Correa[b,c,1], Maja Zagorščak[a], Marko Petek[a], Carissa Bleker[a], Katja Stare[a], Christian Schuy[d], Sophia Sonnewald[d], Kristina Gruden[a,2], and Zoran Nikoloski[b,c,2]

Affiliations are included on p. 10.

Edited by Jens Nielsen, BioInnovation Institute, Hellerup, Denmark; received February 3, 2025; accepted June 19, 2025

Understanding the molecular mechanisms behind plant response to stress can enhance breeding strategies and help us design crop varieties with improved stress tolerance, yield, and quality. To investigate resource redistribution from growth- to defense-related processes in an essential tuber crop, potato, here we generate a large-scale compartmentalized genome-scale metabolic model (GEM), potato-GEM. Apart from a large-scale reconstruction of primary metabolism, the model includes the full known potato secondary metabolism, spanning over 566 reactions that facilitate the biosynthesis of 182 distinct potato secondary metabolites. Constraint-based modeling identifies that the activation of the largest amount of secondary (defense) pathways occurs at a decrease of the relative growth rate of potato leaf, due to the costs incurred by defense. We then obtain transcriptomics data from experiments exposing potato leaves to two biotic stress scenarios, a herbivore and a viral pathogen, and apply them as constraints to produce condition-specific models. We show that these models recapitulate experimentally observed decreases in relative growth rates under treatment as well as changes in metabolite levels between treatments, enabling us to pinpoint the metabolic rewiring underlying growth–defense trade-offs. Potato-GEM thus presents a useful resource to study and broaden our understanding of potato and general plant defense responses under stress conditions.

systems biology | constraint-based metabolic modeling | growth-defence trade-offs | secondary metabolism

Significance

Plants respond to external stresses by redistributing resources from growth- to defense-related processes, often resulting in decreased yields. This results in growth–defense trade-offs, where improvement in one process comes at the cost of the other. Understanding the molecular mechanisms behind such trade-offs can help us design crop varieties with simultaneously improved stress tolerance and yields. To study growth–defense trade-offs in the context of metabolism, we have generated a large-scale reconstruction of potato metabolism, capturing the full known secondary metabolism in a major crop species. The model enables extensive analysis of the interplay between growth and defense processes, as showcased in the study, and is an excellent platform for further development and application.

The challenge of ensuring a secure supply of food for the rising global population is linked to improving not just the yield and quality but also the stress tolerance of major crops (1, 2). Environmental stresses lead to annual losses amounting to billions of euros per crop. Apart from the detrimental effects of abiotic stresses, such as temperature changes, droughts, and floods, biotic stresses lead to yearly losses of up to 80% of crop yield (3–5). In the case of potato, especially damaging are viral infections and herbivore infestations, including Potato virus Y (PVY) (6) and Colorado potato beetle (CPB) (7, 8), respectively. Despite these concerns, the molecular processes underpinning and associating crop yield and defense responses are still not well understood (9, 10). Plants attacked by biotic stressors slow down their growth to preserve molecular resources and direct them for defense purposes, including production of signaling as well as defense compounds (9). Conversely, rapid plant growth to improve accessibility of resources (e.g., when seeking light during germination or due to a crowded environment) is often accompanied by increased susceptibility to pests and pathogens, as growth is prioritized over defense (11). This growth–defense trade-off is a fundamental principle of plant economics, allowing plants to balance growth and defense according to external conditions (9, 10). However, modern agricultural crops, including potato, have been bred to maximize yield- and growth-related traits at the expense of losing useful defense-related traits (12). To this end, improved understanding of the molecular mechanisms behind growth–defense trade-offs is a crucial step toward enhancing breeding strategies that could help design superior crops, combining high yields with the ability to defend against stress (1, 13).

Plant defense responses are often systemic in that they have an effect beyond the infected or damaged tissue (14). They are mediated by complex signaling and regulatory networks which sense and respond to environmental perturbations (15, 16). Hormones, like salicylic acid and jasmonic acid, induce plant resistance mechanisms to either biotrophic pathogens, such as PVY (17, 18), or herbivores, such as CPB (7), respectively. Trade-offs between plant growth and defense typically occur within cellular metabolism, which comprises a complex network of biochemical reactions that synthesize and transform substances into energy and base components necessary for the various cellular tasks (19, 20). Here, plant

Author contributions: J.Z., S.C., K.G., and Z.N. designed research; J.Z., S.C., M.Z., M.P., C.B., K.S., and C.S. performed research; J.Z., S.C., M.Z., M.P., S.S., K.G., and Z.N. analyzed data; and J.Z., S.C., K.G., and Z.N. wrote the paper.

The authors declare no competing interest.

This article is a PNAS Direct Submission.

[1]J.Z. and S.C. contributed equally to this work.

[2]To whom correspondence may be addressed. Email: jan.zrimec@nib.si, kristina.gruden@nib.si, or nikoloski@mpimp-golm.mpg.de.

This article contains supporting information online at https://www.pnas.org/lookup/suppl/doi:10.1073/pnas.2502160122/-/DCSupplemental.

Published August 7, 2025.

growth is mediated by primary, biomass-producing processes that include photosynthesis, respiration, and the synthesis and degradation of carbohydrates, amino acids, and nucleic acids (21), whereas secondary metabolism facilitates the production of a plethora of signaling and defense compounds (so-called specialized metabolites) (22, 23). Lipid metabolism is also a critical subsystem interlinking the growth and defense processes (24), by providing precursors for many molecules in secondary metabolism and signaling pathways.

Growth–defense trade-offs have been studied using classical reverse genetics approaches in Solanaceae (25–27). For instance, overexpression of potato 3-hydroxy-3-methylglutaryl-CoA reductase homologs resulted in dwarfism and highest amounts of sterols (28), and oxylipin-induced growth–defense trade-offs were shown in several plant species, including *Arabidopsis*, tomato, tobacco, and rice (29–31). Simulations of plant growth and development provide another way to study growth–defense trade-offs in specific genotypes and under particular environments, for instance using constraint-based mathematical modeling approaches based on genome-scale metabolic models (GEMs) (32–34). However, in silico analysis of trade-offs requires models that include processes underpinning growth and defense mechanisms, by integrating pathways from primary, secondary, and lipid metabolism. Moreover, there is presently a gap in representing and using the existing knowledge of plant secondary metabolic pathways, as models incorporating secondary pathways [e.g., in rice (35) or *Arabidopsis thaliana* (36)] do not systematically dissect and quantify growth–defense trade-offs. Existing studies of plant metabolic flux trade-offs using constraint-based modeling have been based merely on models of primary metabolism [e.g., *A. thaliana* (37, 38) and condensed representation of metabolism of diverse fruits (39)]. Therefore, to correctly interpret experimental data and study the effects of plant biotic interactions at the molecular level, it is imperative to refine and expand existing metabolic modeling resources to encompass not only the primary but also the full secondary metabolism in an essential food crop system, such as potato.

Here, we present potato-GEM, a metabolic reconstruction of potato leaf metabolism that spans not only all critical primary and lipid metabolic processes, but also adds a full reconstruction of the known potato secondary metabolism. We then perform a general analysis of how secondary metabolite production is linked to plant growth, determining the ability of the model to capture and quantify growth–defense trade-offs and to predict how resource limitation affects these trade-offs. We further process and analyze transcriptomic data from biotic stress experiments on potato leaves, capturing both insect pests (chewing herbivore, CPB) and pathogens (intracellular virus, PVY) interaction characteristics. To connect the enzyme-catalyzed reactions of potato-GEM with the underlying genes, we use the transcriptomic data to constrain reaction upper bounds and build a set of condition-specific models. We find that these models indeed reflect experimental observations of decreased growth under stress conditions and also result in predicted metabolite flux-sums, as proxies of metabolite levels, that match measured relative metabolite levels between control and treated plants. Finally, we perform an in-depth analysis of the condition-specific models using Monte Carlo sampling and pathway enrichment analysis, obtaining further insights into the metabolic rewiring underpinning potato growth–defense trade-offs. Our study thus demonstrates the usefulness of secondary metabolism-expanded models, such as potato-GEM, in the context of constraint-based modeling approaches, to help expand our knowledge and understanding of the molecular principles behind plant stress responses and environmental interactions.

1. Results

1.1. Constructing Potato-GEM by Merging and Curating Multiple Metabolic Modules. To ensure an accurate reconstruction of potato metabolism, we followed a bottom–up approach that avoids issues with gap-filling due to the poor experimentally validated annotation in potato (2.1% of all protein-coding genes). To this end, we first merged the metabolic model of *A. thaliana* core metabolism (AraCore, spanning 549 reactions and 407 metabolites) (32) and the single-tissue model of tomato metabolism, recently updated and expanded in the Virtual Young TOmato Plant (VYTOP, spanning 2,261 reactions and 2,097 metabolites) (33) (*SI Appendix, Supplementary Methods* M1). The rationale for initiating potato-GEM from these models is that tomato is a genetically and metabolically closely related plant from the *Solanaceae* family (40). Moreover, the *Arabidopsis* core metabolism constitutes the set of functionally conserved metabolic pathways across the dicot species (32). During the merging process, we identified an overlap of 298 reactions and 346 metabolites common to both models (Fig. 1*A*). However, the resulting model did not contain a functional secondary metabolism nor was it able to produce necessary lipid-related precursors. To resolve this issue, we further integrated the model with the recently developed Plant Lipid Module (24), identifying an overlap of 279 reactions and 403 metabolites present in the lipid module and the merged AraCore-VYTOP model (Fig. 1*A*). Moreover, we curated 363 reactions from 106 pathways belonging to potato secondary metabolism and 23 related precursor pathways from the MetaCyc-derived Plant Metabolic Network database (41, 42), adding an additional 203 reactions. This resulted in the potato-GEM model spanning 7,092 reactions and 3,801 metabolites (Fig. 1*A*), across 16 unique compartments (Fig. 1*B*: only key compartments are shown since the majority are related to the Plant Lipid Module, Supp. files S1, S2). Compared with the tomato GEM in VYTOP, the number of blocked reactions (i.e., those unable to transport any flux) was reduced over 50-fold (Fig. 1*C*: ratio of blocked reactions 51.4% with VYTOP and 0.9% with potato-GEM), demonstrating the relevance of the bottom–up, well-curated reconstruction procedure.

We next defined a leaf biomass growth reaction to use with potato-GEM metabolic simulations (*SI Appendix, Supplementary Methods* M2). Here, we measured the dry weight to fresh weight ratio as well as the total protein content of potato leaves (*SI Appendix, Supplementary Methods* M3). Additionally, quantitative data for various biomass components, including sugars, organic acids, amino acids, and lipids, were compiled through an extensive review of the literature (24, 33, 45–51). The leaf biomass thus comprised 67 compounds and an additional 122 lipid-related compounds (Fig. 1*D* and *SI Appendix*, Table S1, Supp. file S3). To ensure comparability of predicted growth rates, the component values were further calibrated to a total of 1 g/gDW (44). This was achieved by proportionally increasing their quantities and setting the overall quantity of nucleic acids, for which experimental data were not available, similar to that of proteins (Fig. 1*D*: 14.5% of DW) (33). We then verified that potato-GEM is indeed capable of producing all 189 biomass components under standard phototrophic (light) conditions (*SI Appendix*, Fig. S1.1 and *Supplementary Methods* M4). Moreover, compared with the existing AraCore and VYTOP models, potato-GEM includes a larger number of biomass precursors across multiple component classes (Fig. 1*E*: producing in total 71.8% or 11.7% more biomass precursors if lipids are disregarded, respectively). This supports the model's secondary metabolite-producing functionality.

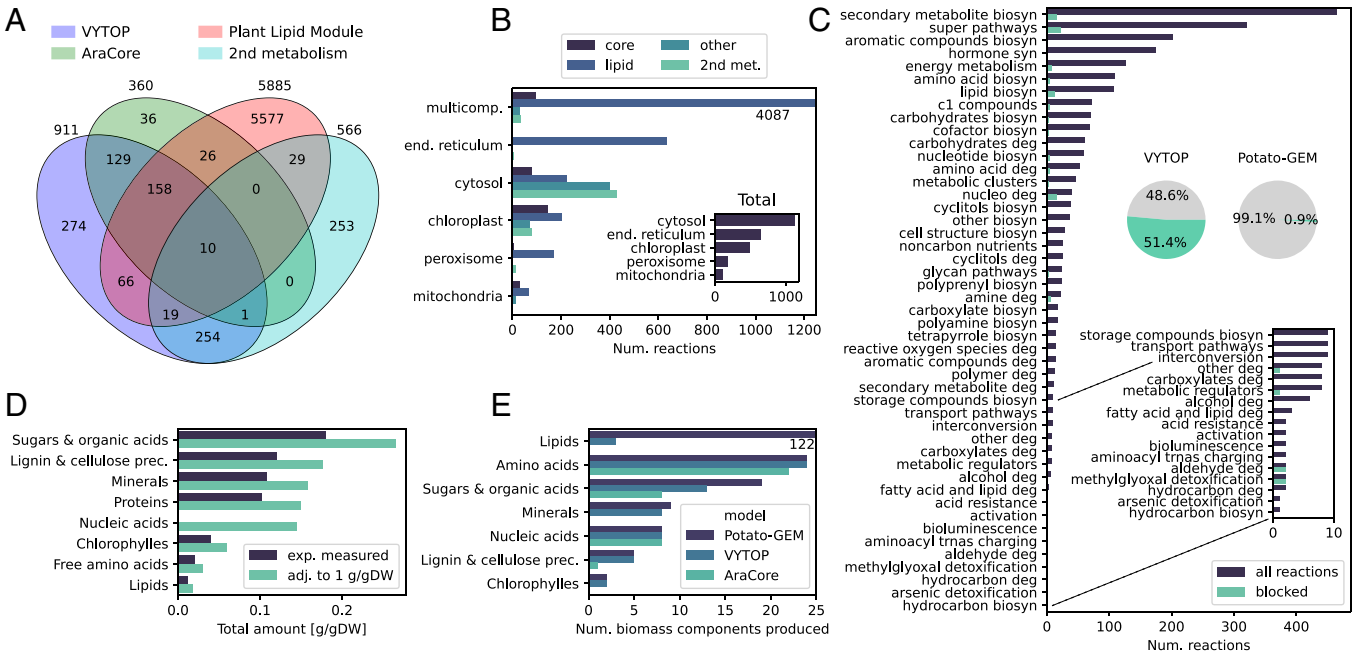

Fig. 1. Constructing potato-GEM by merging and curating multiple modules. (*A*) Venn diagram of the four models that comprise potato-GEM, including AraCore (32), the basic single-tissue model from VYTOP (33), Plant Lipid Module (24) and additional manual curation of secondary metabolism based on the MetaCyc database (42, 43). (*B*) Number of core, lipid, and other primary as well as secondary metabolism reactions across the model's key cellular compartments including multicompartment reactions. *Inset* shows the total number of reactions. (*C*) Depiction of the total number and blocked reactions across the MetaCyc pathway ontology. *Inset* pie charts show the ratio of blocked reactions in VYTOP and potato-GEM. *Lower Inset* shows a zoom in on the values of the bottom 17 pathways. (*D*) Depiction of potato biomass components based on experimentally measured values and after adjustment of total content to 1 g/gDW (44). (*E*) Quantification of the capability to produce biomass precursors across potato-GEM and the existing VYTOP (33) and AraCore (32) models.

Importantly, the reconstruction of secondary metabolism in potato-GEM captures the complete *Solanum tuberosum* secondary metabolism as detailed in the Plant Metabolic Network database (41, 42) (*SI Appendix, Supplementary Methods* M1). It covers the major classes including: i) alkaloids, such as alpha-solanine and alpha-chaconine, calystegines, and tropane alkaloids, ii) phenylpropanoid derivatives, such as flavonoids, coumarins, cinnamates, lignans, and lignins, iii) terpenoids, i.e., carotenoids and mono-, di-, tri-, and sesquiterpenoids, iv) phytoalexins, i.e., resveratrol and capsidiol, and v) hormones, including jasmonic acid, salicylic acid, abscisic acid, auxins, brassinosteroids, cytokinins, ethylene, and gibberellins (Fig. 2*A* and *SI Appendix*, Fig. S1.2). The inclusion of these pathways enables the modeling of the production of defense compounds related to stress response (e.g., hormones), allowing us to study the effects and coupling of growth with secondary metabolite production (19, 52). The complete secondary metabolism spans over 566 reactions in 106 pathways, producing a total of 182 unique secondary metabolites (*SI Appendix*, Figs. S1.2 and S1.3 and Table S2, Supp. file S4).

1.2. Secondary Metabolism Reconstruction Enables Quantifying Growth–Defense Trade-Offs. The refined potato-GEM model enabled us to investigate the coupling (53) between potato growth and stress response modes and to ascertain the possibility of growth–defense trade-offs. To this end, we investigated whether fluxes through secondary pathways and reactions are coupled to biomass production (growth, Fig. 2*B*). Here, the variability of fluxes of the final product-producing reactions in each secondary pathway were evaluated within the optimal biomass space using flux variability analysis (FVA) (54). Different fractions, ranging from 0 to 1, of the optimal relative growth rate were used (Fig. 2*C*). We observed that at the optimal relative growth rate, the majority (88%) of secondary pathways were either inactive, with computed flux ranges of 0 μmol/gDWh^{-1}, or minimally active, with a limited flux range below 0.29 μmol/gDWh^{-1}, occurring for 31 reactions (Fig. 2 *C* and *D*). Furthermore, with a decreasing relative growth rate from the optimum, the majority (>97%) of secondary pathways exhibited proportional increases of their flux ranges (Fig. 2*C*). This was supported by a significant negative correlation (Spearman $\rho = -0.71$, P-value < 10^{-16}, *SI Appendix*, Fig. S2.1) between growth and flux through secondary metabolite production. The results demonstrated that the majority of secondary pathways are thus negatively coupled with the plants' growth objective (Fig. 2*D*: 194 reactions across 103 pathways). In addition, for 99% of these negatively coupled pathways, the predicted flux upper bounds were found to be strongly negatively correlated (Spearman $\rho < -1.0$, P-value < 10^{-16}, *SI Appendix*, Fig. S2.2) with the relative growth rate. The remaining pathways exhibited either nonmonotonic changes (PWY-5751: phenylethanol biosynthesis, one reaction), or were inactive across the whole range of biomass production (two reactions from two pathways, *SI Appendix*, Fig. S2.3). Importantly, an optimal secondary metabolite production was observed at a fraction of 0.6 of the optimal relative growth rate, where the largest amount of secondary reactions and pathways were found to be active (Fig. 2*D*: 99% and 98%, respectively).

The observed negative coupling between growth and secondary metabolism (Fig. 2*C*) suggested that a growth–defense trade-off is occurring with these pathways. Therefore, to identify secondary metabolites that most affect the biomass objective function, we further computed shadow prices for demand reactions producing a secondary metabolite of interest (55) (*SI Appendix, Supplementary Methods* M4). These demonstrate how much a unit increase of flux through secondary pathway (defense) production decreases the flux through the biomass reaction (growth), which can be interpreted as a growth–defense trade-off factor (Fig. 2*B*). We also implemented and applied a procedure to determine the energetic cost of secondary metabolites (*SI Appendix, Supplementary Methods* M4). In line with expectations, we found that the shadow prices

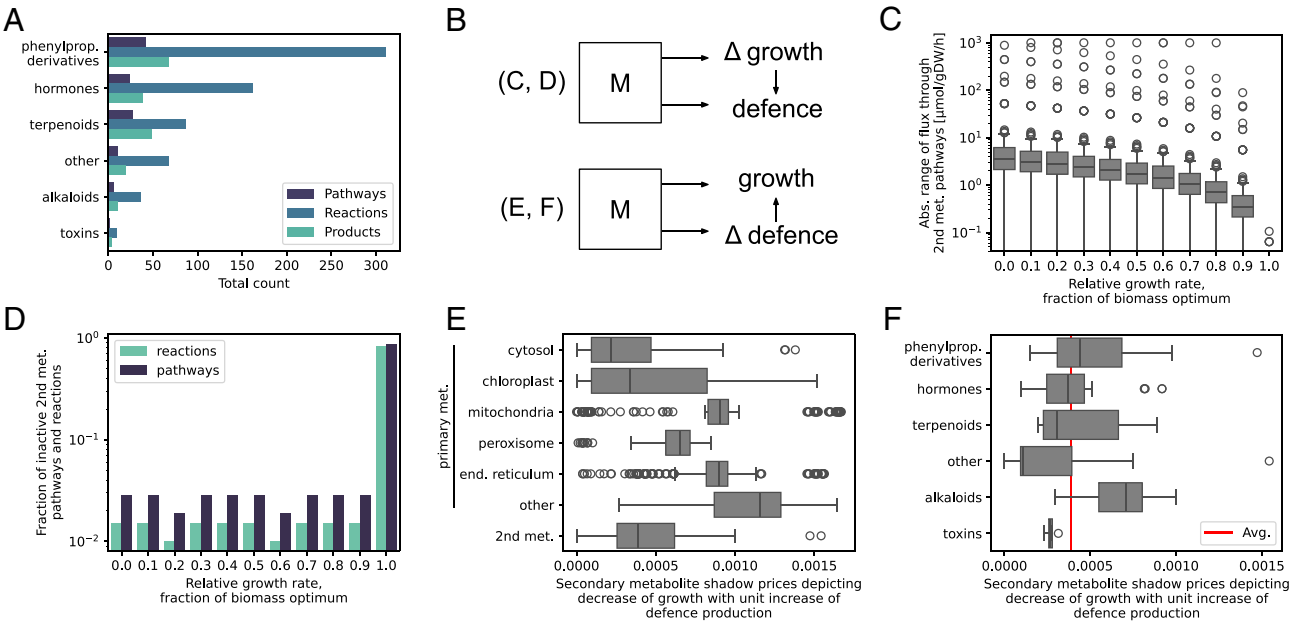

Fig. 2. Secondary metabolism reconstruction enables quantifying growth–defense trade-offs. (*A*) The number of reactions, pathways, and products across secondary metabolism classes in the reconstruction. (*B*) Schematic depiction of the studied growth–defense trade-off relationships by either observing the effects of growth limitation on defense activation (as depicted in panels C and D) or vice versa (panels E and F). (*C*) Depiction of predicted growth–defense trade-off capabilities as the absolute range of flux through secondary metabolic pathways in response to the varying ratio of optimal biomass production in FVA. (*D*) Ratio of inactive secondary pathways and reactions in response to the varying ratio of optimal biomass production in FVA, showing that the majority of secondary pathways are coupled with growth and exhibit growth–defense trade-offs. (*E*) Distribution of shadow prices of primary and secondary metabolites, depicting the decrease of biomass flux per unit increase of flux through different parts of metabolism. (*F*) Distribution of shadow prices across secondary metabolite classes. The red line denotes median value across the whole secondary metabolism.

were significantly and strongly correlated (Spearman ρ = 0.99, P-value < 10^{-16}) with computed costs of metabolite production as well as with metabolite molecular weights (Spearman ρ = 0.75, P-value < 10^{-16}, *SI Appendix*, Fig. S2.4), demonstrating the validity of the model. On average, across all coupled secondary pathways, we observed a 3.9 × 10^{-4} decrease of biomass flux with a unit increase of secondary metabolite production (Fig. 2*E*). Moreover, we found that this growth–defense trade-off factor remains on average relatively equal across different secondary metabolite classes (Fig. 2*F*). The exception was with alkaloids, exhibiting the largest trade-off factor of 7.1 × 10^{-4}. This was almost twofold and significantly (Wilcoxon rank-sum test P-value = 0.002) larger than with the remaining secondary metabolism classes, likely due to the large costs of their synthesis (56). Compared to primary metabolism, the growth–defense trade-off factor of secondary metabolites was almost twofold and significantly (Wilcoxon rank-sum test P-value = 1.3 × 10^{-11}) higher than shadow prices obtained with cytosolic primary metabolites (Fig. 2*E*: ~10^{-5}). Average shadow prices for demand reactions of primary metabolites in the chloroplast were however relatively similar to those of secondary metabolites (Fig. 2*E*: 3.4 × 10^{-4}), and further increased across the remaining compartments due to specialized metabolism, such as highly costly lipid production (57). Considering the distribution of core metabolism mostly among the cytosol and chloroplast (Fig. 1*B*: ~78% of reactions), the results suggest that defense activation under stress requires a relatively higher amount of resources (Fig. 2*E*: up to twofold more) than the general rewiring of core metabolism.

1.3. Exploring the Effects of Resource Limitation on Growth and Defense. We next explored the possibility that resource constraint is a primary reason for the inverse growth–defense relationship, whereby providing more resources would reduce growth–defense trade-offs and allow plants to simultaneously grow and defend themselves (10, 58). To this end, we proportionally limited or increased the availability of key resource inputs: CO_2, light, nitrogen, or a combination of all three (Fig. 3*A* and *SI Appendix, Supplementary Methods* M4). We observed proportional decreases in the predicted growth rates when limiting resources, reaching no growth when resources were completely withdrawn (Fig. 3*B*: note that a resource ratio of 1 is used to denote resource consumption at the optimal relative growth rate). Conversely, as expected, no change in growth was observed when increasing resource availability above a resource ratio of 1 (*SI Appendix*, Fig. S3.1). The secondary metabolite production capacity decreased significantly (Wilcoxon rank-sum test P-value < 10^{-16}, measured between the resource ratio of 1 and 0) and proportionally with varying CO_2 and light availability (Fig. 3*C*). However, with nitrogen limitation, the defense response increased by over twofold for a nitrogen ratio between 1 and 0 (Wilcoxon rank-sum test P-value < 0.002). This further unlocked the model's optimal secondary metabolite production reached at a fraction of 0.6 of the optimal relative growth rate within the given constraints. Increasing resource availability, on the other hand, did not lead to an increased secondary production capacity (*SI Appendix*, Fig. S3.2). The results suggest that under actual in situ conditions, where plants do not grow at the metabolic optimum (as depicted in Fig. 3*C*), access to more resources could indeed decrease growth–defense trade-offs by allowing plants to simultaneously grow and defend themselves (10). Moreover, the availability or limitation of certain key resources, such as nitrogen, can also strongly affect the defense capacity and is a point of possible improvement.

1.4. Capturing Biotic Stress Responses with Transcriptomics Data. Our next aim was to investigate a range of common potato biotic stress scenarios and the growth–defense trade-offs that they elicit. To this end, we performed a transcriptomics experiment based on the herbivore attack of potato leaves with the CPB and complemented it with previously published data on the pathogen interaction with the PVY (6) (Fig. 4*A*). Briefly, plants were exposed

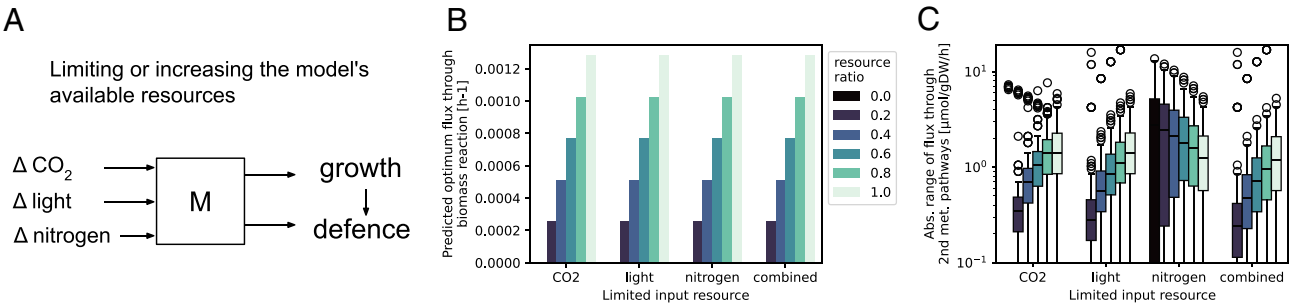

Fig. 3. Exploring the effects of resource limitation on growth and defense. (*A*) Schematic depiction of the analysis of resource limitation or expansion, where the key resources CO_2, light, and nitrogen were varied within a range of 0 to 1 relative to the resource consumption flux obtained at an optimal growth rate of 1. (*B*) Effect of resource limitation on the predicted relative growth rate (biomass optimum). (*C*) Effect of resource limitation on the range of secondary metabolite production (defense), computed at the fraction of 0.6 of the optimal relative growth rate to observe the largest amount of possible active secondary metabolism.

to two beetles per leaf for 30 min, and 24 h post infection the leaf region surrounding the damaged part was sampled in parallel with noninfested leaves (control) and processed for RNA-Seq (*SI Appendix, Supplementary Methods* M3 and M54). In the previously published PVY experiment (18), leaves were inoculated with PVY and tissue immediately surrounding the site of viral multiplication was sampled when the hypersensitive resistance response was fully established (4 d after inoculation). This was performed in parallel with control noninoculated leaves tissue, and all tissues were then processed for RNA-Seq (*SI Appendix, Supplementary Methods* M5). Biological triplicates were analyzed per treatment, resulting in a total of 12 samples.

Nonmetric multidimensional scaling analysis of transcript counts indicated clear separation among treated and control samples in both experiments (Fig. 4*B* and *SI Appendix*, Fig. S4.1 and *Supplementary Methods* M5). We also observed significant correlation (Spearman $\rho = 0.77$, P-value < 10^{-16}) of transcript counts among the control samples of both experiments (*SI Appendix*, Fig. S4.2). While correlation analysis among all 12 samples showed a clear distinction between PVY control and treatment samples, this was not observed with CPB samples (Fig. 4*C*). The CPB experiment also captured a smaller number of differentially expressed genes (325 DEGs), compared to the PVY experiment (9,289 DEGs) (Fig. 4*D*, Supp. file S5). These differences were likely due to the shorter CPB exposure time and thus milder observed defense response than with PVY (18). Nevertheless, further DEG and enrichment analysis using plant specific MapMan ontology terms (59) showed i) an increase in hormonal production, specifically salicylic acid with PVY (17) and jasmonic acid with CPB (8, 62), which are known signaling cascade regulators of the specific biotic stresses, ii) general upregulation of multiple secondary pathways, including those belonging to glycoalkaloid (63), phenylpropanoid (64, 65) and terpenoid classes (66), iii) lowered photosynthetic activity with PVY (67), iv) upregulated sucrose degradation factors with PVY likely due to increased sucrose accumulation (65), as well as v) downregulation of biotic stress response-related factors due to an overactivated signaling response (Fig. 4*E*, Supp. file S6) (16). This suggested that known responses as a consequence of biotic stress and growth–defense trade-offs were indeed captured in both experiments (18).

1.5. Transcriptome-Constrained Models Recapitulate Reduced Growth in Stress Response. To further study the characteristics of biotic interactions, we next constructed models constrained by the transcriptomics data (Fig. 5*A*). To this end, we first annotated model reactions with gene protein reaction (GPR) associations, which were obtained from the MetaCyc-derived Plant Metabolic Network database (41) (*S. tuberosum* subset) as well as by translating GPRs with *Arabidopsis* gene identifiers from the Plant Lipid Module (24) and AraCore (32) modules (*SI Appendix, Supplementary Methods* M6). Here, orthologous genes between *Arabidopsis* and potato were identified according to Plaza v5.0 (68) orthologs using clustering algorithms as well as BLAST reciprocal best hit search (69, 70). This yielded a set of 2,173 potato gene identifiers and resulted in 3,474 reactions (49%) annotated with GPR associations comprising, on average, two unique gene identifiers (Fig. 5*B* and *SI Appendix*, Fig. S5.1 and Table S3). As expected, better coverage of GPR-annotated reactions of 64% was achieved with the core metabolism compared to a ~50% coverage of both the lipid and secondary metabolism (Fig. 5 *B*, *Inset*). However, secondary metabolism reactions were annotated with GPR associations that comprised significantly more unique gene identifiers than those in primary metabolism (Wilcoxon rank-sum test P-value < 3×10^{-13}), with a 1.5-fold higher number of genes on average (Fig. 5*C*). Within secondary metabolism, apart from precursors exhibiting the highest coverage (85%), terpenoid, toxin, and phenylpropanoid derivative classes achieved a better than average coverage of 49% or higher (Fig. 5*D*).

Next, we integrated the transcriptomics data with the potato-GEM model, by evaluating GPR associations based on the provided transcriptomic measurements to constrain the model's upper bounds of flux across reactions (*SI Appendix, Supplementary Methods* M5). This resulted in 12 transcriptomics-constrained models, one for each replicate of the data treatment (control and treated) and experiment type (CPB and PVY; see Fig. 4). An initial 14,404 and 19,367 transcripts from the CPB or PVY experiment, respectively, were mapped to GPR associations across 3,140 and 3,207 reactions, respectively (*SI Appendix*, Fig. S5.2). Compared to the overall proportion of essential reactions in the model of 6.2% (439), without which the model cannot produce the target biomass (71), a significantly (Fisher's exact test P-value = 1.1×10^{-4}) larger proportion of ~8.6% were found to be GPR-annotated (*SI Appendix*, Fig. S5.1: 267 and 277, respectively). We observed that the variability of the upper bounds of the CPB dataset constrained models differed significantly (Wilcoxon rank-sum test P-value < 10^{-16}) across treatments (*SI Appendix*, Fig. S5.3). Here, models corresponding to treated samples exhibited an average 2.5-fold increase in variability of upper bounds compared to controls. However, this was not the case with the PVY dataset, where the variability remained approximately equal between treated and control models. Moreover, the transcriptomics-constrained reactions were found to comprise the full range of pathways covering 96% of the key cellular processes as existing in the original unconstrained model (Fig. 1*C* and *SI Appendix*, Fig. S5.4).

Finally, we observed that under both biotic stress scenarios, the predicted relative growth rates (*SI Appendix, Supplementary Methods* M4: phototrophic regime as applied in the experimental setup) with the constrained models of treated plants were on

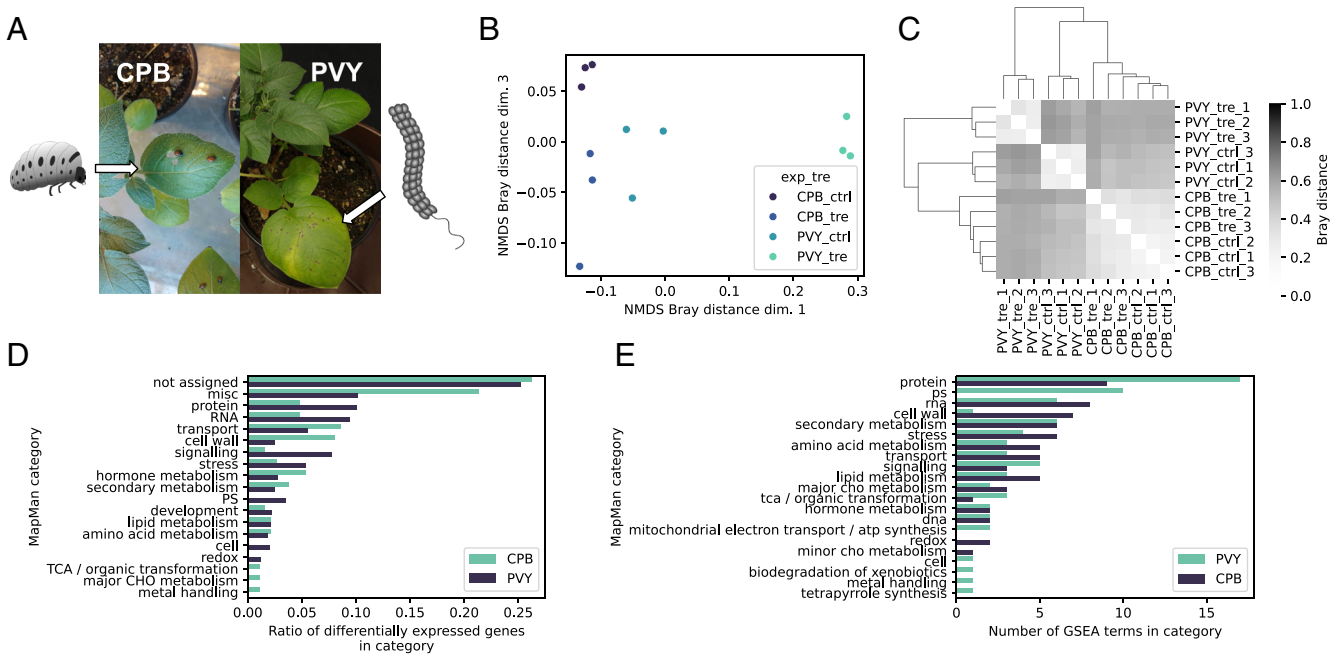

Fig. 4. Capturing biotic stress responses with transcriptomics. (*A*) Schematic depiction of biotic stress transcriptomics experiments with CPB and PVY. (*B*) Principal-coordinate analysis of Bray–Curtis dissimilarity between transcript counts across experiments and treatments. (*C*) Heatmap and dendrogram visualization of hierarchical clustering on Bray–Curtis dissimilarity between sample replicates across experiments and treatments. (*D*) Ratio of differentially expressed genes (DEGs) (BH-corrected *P*-value < 0.05 and abs(log2FC) > 2) belonging to a MapMan (59, 60) category vs. the total number of DEGs across experiments. Ratios above 0.025 shown. (*E*) Transcriptomics responses on the level of pathways. MapMan-defined pathways (59, 60) enriched with differentially regulated genes were calculated using Gene Set Enrichment Analysis (61) (BH-corrected *P*-value < 0.05).

average 75% lower than that of controls (Fig. 5*E*). Here, 39.6% of the optimal growth rate was observed with CPB and 9.8% with PVY, respectively. This is in line with experimental findings, where growth rates under biotic stress treatments have generally been found to be lower compared to controls (72, 73). To further validate model predictions, we applied randomized Monte Carlo sampling using the Artificial centered hit and run algorithm (74) (*SI Appendix, Supplementary Methods* M4). We ensured that growth–defense trade-offs were accurately captured in the sampling procedure by using appropriately set reaction bounds. These

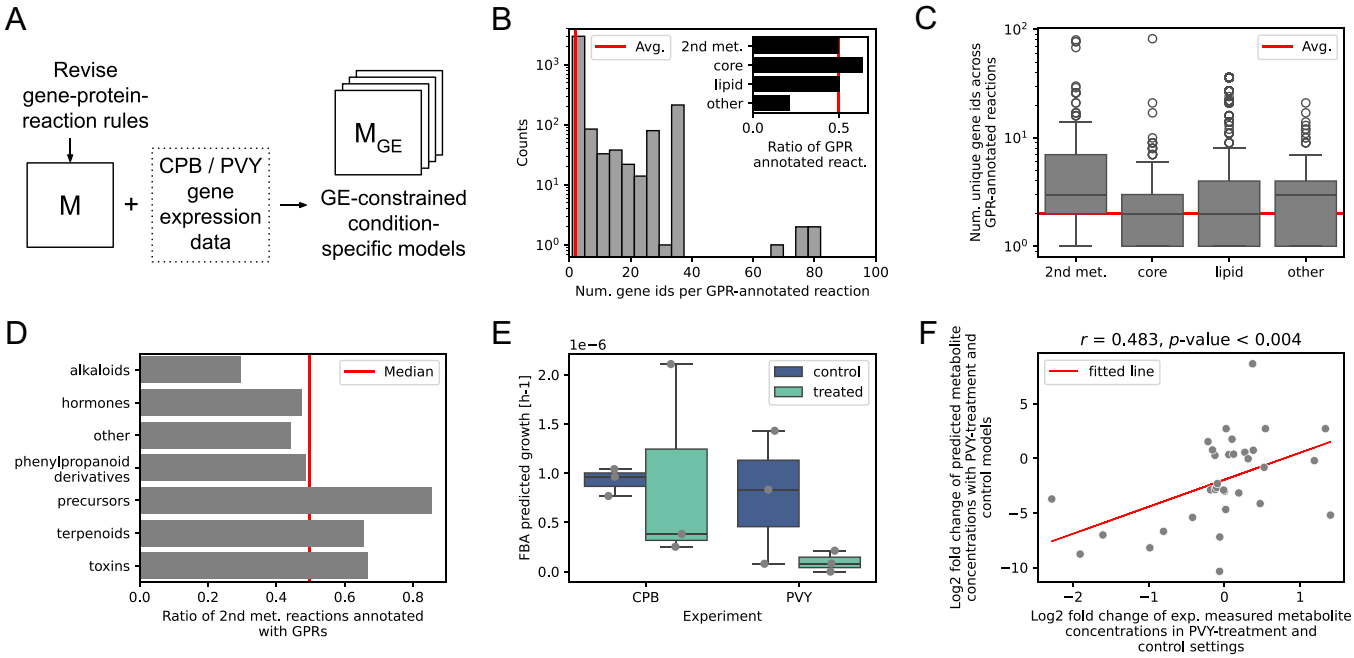

Fig. 5. Transcriptome-constrained models recapitulate reduced growth in stress response. (*A*) Schematic depiction of the procedure to construct a set of CPB- and PVY-transcriptome constrained models. (*B*) Number of gene identifiers present in GPR associations across GPR-annotated reactions. The red line denotes an average value of 2. *Inset* depicts the ratio of GPR-annotated reactions across the general metabolic types. (*C*) Number of gene identifiers present in GPR associations of GPR-annotated reactions across the general metabolic types. The red line denotes the average value. (*D*) Ratio of GPR-annotated reactions across secondary metabolism classes. The red line denotes the average value. (*E*) Predicted biomass production with the transcriptome constrained models under a phototrophic regime. (*F*) Validation of model performance: Correlation analysis of predicted metabolite flux-sums (as proxies for metabolite levels) from randomized sampling results using PVY transcriptomics-constrained models and published relative metabolite levels from metabolomics experiments upon potato PVY infection (65).

were obtained from FVA performed over a range of fractions of the biomass optimum, between optimal secondary metabolism production (at the fraction of 0.6 of the optimal relative growth rate) and optimal biomass production (fraction of 1; see Fig. 2*C*). Additionally, we considered that trade-offs are related to known hormone responses and mediated by extensive signaling cascades (15) that are not the part of the present metabolic model. We thus imposed that the models of nonstressed control conditions produce no jasmonic acid with CPB and no salicylic acid with PVY, respectively, based on experimental and published observations (8, 17, 62). Comparing the flux sampling results and published potato metabolomics data 3 d post PVY infection (65), we found a significant correlation (Spearman ρ = 0.48, *P*-value < 0.004) between log-transformed measured relative metabolite levels and predicted metabolite flux-sums (as proxies for metabolite levels) (75, 76) between treatment and control for 33 key metabolites present in the models (Fig. 5*F* and *SI Appendix*, Table S4). Therefore, our results indicated that the transcriptomics-constrained models result in predictions that are well supported by experiments (36, 77), supporting the usefulness of these models to further study biotic stress-induced growth–defense trade-offs in the context of metabolism.

1.6. Exploring the Mechanisms of Growth–Defense Trade-Offs under Biotic Stress. We next set out to perform a large-scale treatment-specific analysis of metabolism to obtain a global picture of metabolic responses under biotic stress. To this end, we used the randomized Monte Carlo sampling results described above (Fig. 6*A* and *SI Appendix, Supplementary Methods* M4). We performed differential flux analysis to identify reactions that exhibited significant (Kolmogorov–Smirnov test BH-corrected *P*-value < 0.05) and over twofold differences in flux values between treatment and control conditions, on average (*SI Appendix, Supplementary Methods* M7, note that replicates were pooled for these computations). In relation to the fold-change cutoff used, which varied from 2 to 10, the analysis revealed between 2,343 and 644 (33% and 9%) differential reactions with CPB, and between 3,402 and 1,751 with PVY (48% and 25%), respectively (Fig. 6*B* and *SI Appendix*, Fig. S6.1). With both experiments, the fluxes of differential reactions were on average 90% lower in treatment models compared to control ones, which was likely due to a higher number of downregulated reactions compared to up-regulated ones observed with both experiments (Fig. 6*B*). This was especially prominent with PVY, where the number of downregulated reactions was fourfold higher. Despite this, fluxes across secondary metabolism increased by ~1.5-fold between treatment and control models in both experiments (*SI Appendix*, Fig. S6.2 and Table S5).

To determine the pathways comprising the reactions exhibiting differential fluxes across conditions, we next performed enrichment analysis of metabolic subsystems at the level of Biocyc ontologies (Fig. 6 *C*–*E* and *SI Appendix*, Fig. S6.3 and Tables S5 and S6). We found that CPB models were significantly (Fisher's exact test BH-corrected *P*-value < 0.05) enriched in 21 BioCyc pathways, whereas PVY models spanned 28 pathways (Fig. 6 *D* and *E*). In both experiments, multiple secondary metabolism pathways displayed differential fluxes (Fig. 6*C*: a total of 14 secondary and 3 precursor pathways with CPB, and 15 secondary and 5 precursor pathways with PVY, respectively), with a ~twofold higher number of upregulated secondary pathways than downregulated ones. Interestingly, we observed that different secondary pathways were differentially regulated under the different biotic stresses (Fig. 6*D*). For instance, viral infection caused the induction of hormonal pathways, including salicylic acid and cis-zeatin, as well as multiple terpenoids, phenylpropanoids, and alkaloids. Insect feeding also led to the increased synthesis of multiple stress-responsive hormones, including jasmonic acid, trans-zeatin and abscisic acid, as well as increased terpenoid production. Indeed, besides salicylic and jasmonic acid, cytokinins are also known to be involved in plant stress responses, besides their main role in development (78, 79). With both biotic stresses, terpenoid precursors were induced in line with the observed terpenoid production, known to protect plants from both viral infections and herbivores by inducing indirect defenses and priming neighboring plants (80). On the other hand, specific growth-promoting hormones were observed to be downregulated (Fig. 6*D*: brassinolides and gibberellins). Interestingly, apart from downregulation of certain resource-related primary metabolic pathways, energy-related metabolism was induced in PVY models (Fig. 6*E*).

Next, we analyzed the correlation between the sampled fluxes of the enriched secondary and primary pathways under the biotic stress conditions. Fluxes were summed over the respective reactions per pathway to obtain the total pathway flux per experiment-treatment combination (*SI Appendix, Supplementary Methods* M7). Indeed, significant correlations ($|\text{Spearman } \rho| > 0.11$, $P\text{-value} < 3.6 \times 10^{-4}$) were found among almost all pathways (Fig. 6 *F* and *G*: secondary vs. primary metabolism pathways shown depicting growth–defense trade-offs). We further observed that specific groups of pathways demonstrated similar growth–defense trade-off patterns in the context of secondary vs. primary pathway flux correlations (*SI Appendix*, Figs. S6.4 and S6.5). For instance, with the CPB models, four groups of secondary metabolism-related pathway responses were identified using clustering based on the cosine distance (Fig. 6*F* and *SI Appendix*, Fig. S6.4 and *Supplementary Methods* M7). Here, we observed a group showing strong negative correlation (Spearman $\rho < -0.76$, $P\text{-value} < 10^{-16}$) between fluxes in the induced stress-related hormone pathways (jasmonic and salicylic acid) as well as terpenoids and their precursors, and the downregulated primary pathways (*SI Appendix*, Table S7). Similarly, four distinct groups were observed with PVY (Fig. 6*G* and *SI Appendix*, Fig. S6.5), showing strong positive correlation (Spearman $\rho \geq 0.69$, $P\text{-value} < 10^{-16}$) between upregulated hormonal and secondary pathways and the induced energy metabolism, and negative correlation (Spearman $\rho \leq -0.42$, $P\text{-value} < 10^{-16}$) between these secondary pathways and downregulated primary pathways (*SI Appendix*, Table S8). Conversely, the downregulated growth-related hormones were negatively correlated (Spearman $\rho \leq -072$, $P\text{-value} < 10^{-16}$) with energy metabolism and positively (Spearman $\rho \leq -0.44$, $P\text{-value} < 10^{-16}$) with the remaining primary pathways. This showcases how the specific primary metabolic rewiring, which underlies secondary defense activation and production under stress conditions, can be pinpointed, and suggests the existence of distinct groups of metabolic trade-offs useful for further study.

2. Discussion

In the present study, we asked whether we can explain and quantify plant growth–defense trade-offs through metabolic flux signatures obtained by constructing and analyzing a sufficiently comprehensive and accurate model of primary and secondary metabolism in the major crop plant, potato. To this end, we developed and applied potato-GEM, a GEM constructed by merging multiple models (32, 33) and modules (24) (Fig. 1*A*), and includes a reconstruction of the full potato secondary metabolism according to the Plant metabolic network (41) MetaCyc database (42) (Fig. 2*A*). We demonstrated that through its comprehensiveness and the secondary metabolism reconstruction, the model enables exploring the

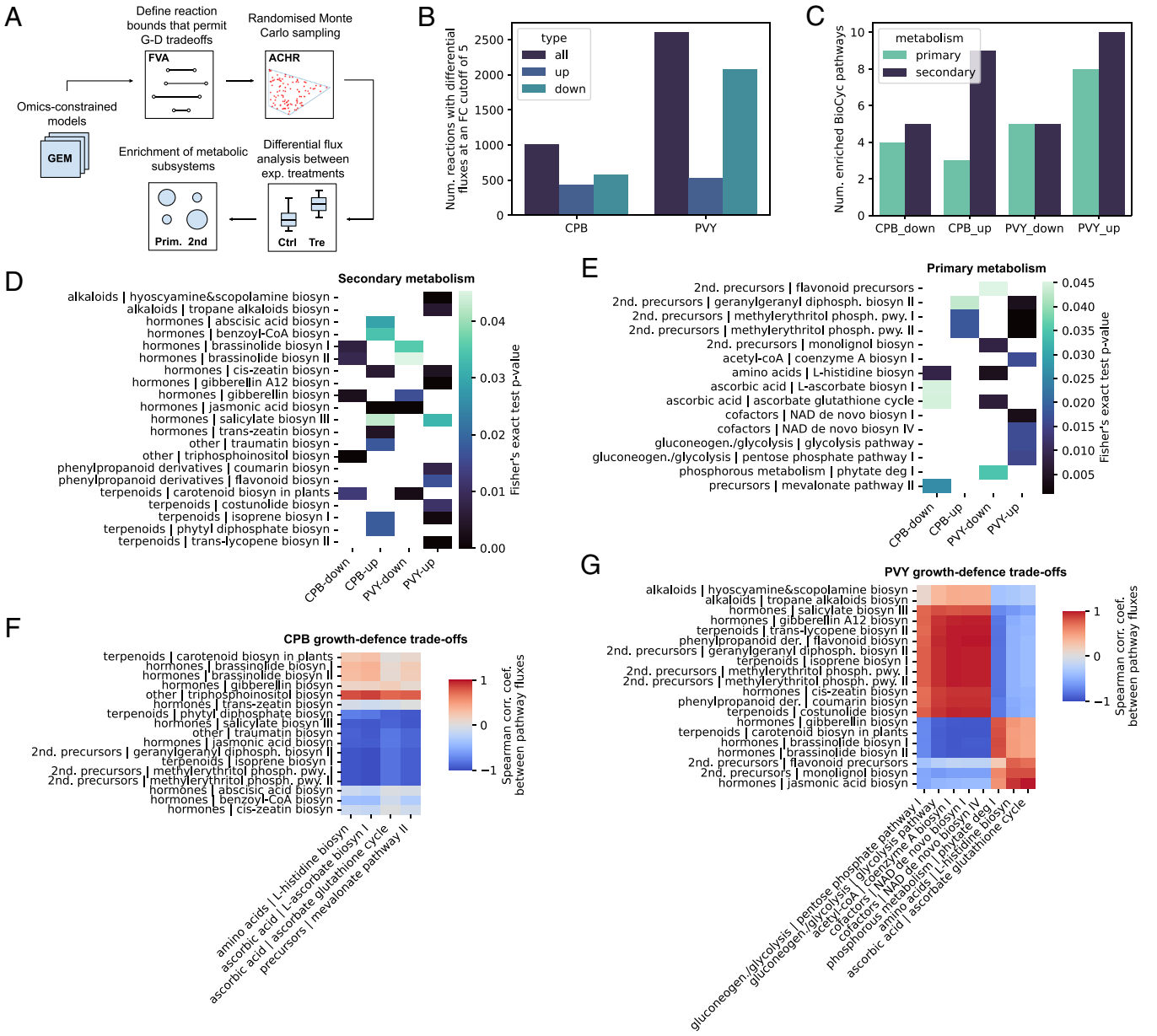

Fig. 6. Exploring the mechanisms of growth–defense trade-offs under biotic stress. (*A*) Schematic depiction of the randomized sampling procedure applied to investigate the enrichment of metabolic subsystems among biotic stress treatment and control models. (*B*) Number of identified reactions with differential fluxes at a fold-change cutoff of five (Kolmogorov–Smirnov test BH-corrected *P*-value < 0.05). Upregulated (up), downregulated (down), and total (all) number of reactions depicted separately. (*C*) The number of significantly (Fisher's exact test BH-corrected *P*-value < 0.05) up- and down-regulated BioCyc pathways according to differential reactions. (*D*) Heatmap of secondary metabolism BioCyc pathways significantly (Fisher's exact test BH-corrected *P*-value < 0.05) enriched in differential reactions (*SI Appendix*, Table S6). (*E*) Heatmap of primary metabolism BioCyc pathways significantly (Fisher's exact test BH-corrected *P*-value < 0.05) enriched in differential reactions. (*F* and *G*) Correlations between total fluxes of the enriched (Fisher's exact test BH-corrected *P*-value < 0.05) secondary vs. primary pathways, demonstrating growth–defense trade-offs, with the (*F*) CPB and (*G*) PVY models. Dendrograms depicting grouping of profiles shown in *SI Appendix*, Figs. S6.4 and S6.5, Spearman correlation coefficient used (n = 1,000 samples).

principles of plant growth–defense trade-offs in the context of metabolism and under biotic stress.

The bottom–up approach that we applied to construct potato-GEM, leveraging existing knowledge and careful curation, contrasts a top–down approach, where genome-wide metabolic networks are constructed automatically from genome annotations and reliant on gap-filling prior to further curation (71). This avoids the need of relying on external databases or models from nonrelated organisms in gap-filling, as is frequently the case in modern metabolic reconstructions, which pollute the models with reactions from nonrelated organisms (81). We leveraged the information from three state-of-the-art resources on metabolism from higher plants, namely a AraCore (32), providing a highly curated model for central metabolism in the model C3 plant, *A. thaliana*, VYTOP (33), providing a larger metabolic model tailored to tomato, and the Plant Lipid Module (24), that offers the largest and most detailed model of plant lipid metabolism (Fig. 1*A*). All of these models have been extensively manually curated and tested in a number of studies. Further inspection pointed to the need for careful manual curation of the diverse pathways of secondary metabolism, that are only partly included in a few models dedicated to these pathways (35, 36, 82). Thus, up to date, none of the existing plant metabolic models offers a detailed inclusion of the full complement of well-characterized pathways of hormonal biosynthesis or secondary metabolism (Fig. 2*A* and *SI Appendix*, Table S2). Moreover, we showed that the number of GPR-annotated

reactions is proportional to the model size, following the trend defined by a variety of published plant models (*SI Appendix*, Fig. S5.1 and Table S9). The number of blocked reactions was however the lowest among all the compared published models (Fig. 1*C* and *SI Appendix*, Table S9). Finally, potato-GEM was validated with experimental measurements, by i) recapitulating stunted potato growth under stress (72, 73) (Fig. 5*E*), ii) recapitulating relative metabolite levels under PVY infection (65) (Fig. 5*F*), and iii) demonstrating correlations between computed metabolite costs and metabolite molecular weights (*SI Appendix*, Fig. S2.5).

Similarly to growth (32, 33), plant responses to abiotic and biotic stress comprise a large set of cellular processes (15, 16, 52). In contrast to targeted in planta experimental research that may be limited to studying merely a subset of different molecular responses at once (9), in silico mathematical modeling of cellular processes such as metabolism (24, 32) and signaling (15, 16) enables us to jointly capture and examine the full range of cellular responses. The potato-GEM model thus allowed us to observe, explore, and interpret the rewiring of plant metabolism from growth to defense-driven responses. The analysis of growth–defense trade-offs was performed in two ways. First, we directly probed the model using flux balance analysis (FBA) and FVA (54, 83) (Figs. 2 *B* and 3*A*), either by i) decreasing the relative growth rate (fraction of biomass optimum) and observing how defense pathways are unlocked (Fig. 2 *C* and *D*), ii) computing shadow prices for demand reactions producing secondary metabolites to determine the effects of the production of these metabolites on growth (Fig. 2 *E* and *F*), or iii) testing the effect of limiting different key input resources on the growth–defense trade-offs (10, 58) (Fig. 3 *B* and *C*). Second, we constrained the model according to experimental gene expression measurements under biotic stress (18) (Fig. 4) and then analyzed model predictions by performing i) FBA (Fig. 5*E*), ii) metabolite flux sums and iii) a sequential combination of FVA and randomized sampling followed by differential flux analysis and pathway enrichment analysis (74, 84) (Fig. 6).

As a result of the first approach, we found that the effects of decreasing the relative growth rate (flux through the biomass reaction) were significantly negatively correlated with increasing flux through secondary pathways (Fig. 2*C*), enabling us to quantify specific general principles of growth–defense trade-offs. Specifically, we identified that the largest number of defense-related secondary metabolism pathways are active at a decrease of ~40% of the potato relative growth rate (Fig. 2*C*: fraction of biomass optimum of 0.6). Further, compared to primary metabolism, we found that the secondary metabolism response involves more costly metabolic processes, based on measuring the effect of perturbing secondary metabolite production (Fig. 2*E*: unit change flux through secondary pathways) on growth (flux through biomass reaction). The cost of diverted resources is also, on average, approximately equal across the secondary metabolite classes (Fig. 2*F*). Indeed, it is known that due to the costliness of diverting energy and resources away from key processes, such as growth and reproduction (85), cells employ multiple strategies to lower the high metabolic costs of defense (23). Apart from fine-tuning secondary metabolite production via gene expression, metabolite multifunctionality, and effective recycling (23), balancing the objectives between biomass or defense production is a key cellular strategy defined by the spectrum of resistance and tolerance of the underlying plant genotype (85). Last, we found that resource limitation has a profound effect on growth–defense trade-offs, effectively decreasing defense rewiring due to a lack of resources (Fig. 3*C*). This supports the existing resource allocation theory (58, 86), whereby resource constraints are a primary reason for the inverse growth–defense relationship. Namely, since plants typically do not optimize merely the growth objective and thus do not necessarily grow at the metabolic optimum, they can find themselves somewhere between the minimum and maximum modeled growth rate (Fig. 3*B*: 0 to 1 relative growth rate). Thus, providing more resources, such as increasing specific nutrients and/or light (Fig. 3*C*), would reduce growth–defense trade-offs, resulting in more secondary metabolism activation at a higher growth rate and thus allowing plants to simultaneously grow and defend (10). On the other hand, the availability of certain nutrients might also have an opposite effect, as was found for nitrogen (Fig. 3*C*), suggesting that the level of such resources needs to be further fine-tuned with respect to the system state in the resource-growth–defense spectrum.

To apply potato-GEM to study growth–defense trade-offs under biotic stress, we first performed and processed transcriptomics experiments exposing potato leaves to CPB (this study) and PVY (18), respectively (Fig. 4*A*). According to differential gene expression and pathway enrichment analyses of the transcriptomics data, both experiments captured the full expected response of their corresponding stresses (Fig. 4 *D* and *E*), despite the CPB experiment characterizing a more early stage of the stress response than was the case with PVY (18). By revising the potato-GEM gene-protein-reaction (GPR) associations that link gene expression and reactions (Fig. 5 *A* and *B*), we constrained reaction upper bounds according to the measured gene expression levels (87, 88). This resulted in a set of condition-specific models, which, when predicting optimal growth rates using FBA, predicted decreased growth under biotic stress compared to controls (Fig. 5*F*), in accordance with published experimental observations. For instance, in a study measuring the effect of CPB damage on potato growth rates in different plant growth stages, damage during both the vegetative and tuber-bulking phases led to decreased haulm and tuber growth rates (73). Similarly, PVY infected plants, grown from infected seed tubers, displayed slower growth rates and lower tuber yields compared to plants grown from noninfected tubers (72). Enzyme-constrained models offer an improvement over the present approach, and allow accounting for posttranscriptional regulation influencing metabolic fluxes beyond transcriptomics data constraints (89). However, their usage requires integration and availability of turnover numbers, which are presently not available with a great coverage for potato.

Finally, we performed Monte Carlo sampling of the condition-specific models. Using PVY infection metabolomics data (65), we showed that the relative changes of computed metabolite flux-sums, which served as proxies for metabolite levels, were significantly correlated with relative measured metabolite levels between treatment and control (Fig. 5*F*). By further differential flux and pathway enrichment analysis (Fig. 6*A*), we observed a large and significant fraction of reactions exhibiting differential fluxes between controls and biotic-stress treatments with both experiments (Fig. 6 *B* and *C*). These differential flux reactions were enriched both in primary metabolic pathways as well as those involved in secondary metabolite and hormone production (Fig. 6 *D* and *E*), in line with previous observations (8, 90). Furthermore, analysis of the correlations among the sampled secondary and primary pathway flux states enabled us to directly investigate metabolic growth–defense trade-offs and how different defense pathways are activated or deactivated in accordance with specific primary metabolic changes under biotic stress (Fig. 6 *F* and *G*). These concerted metabolic changes point to interesting areas of further study as they enable the development of strategies to control or alleviate multiple growth–defense trade-offs possibly by

perturbing primary metabolic responses. Apart from this, our results demonstrated how metabolic modeling is a useful expansion of transcriptomics analysis and a complement to the analysis of immune signaling network responses (8, 15, 18), as it can highlight potentially different underlying aspects of growth–defense mechanisms that are not clearly observable at the gene regulatory or molecular signaling levels (91, 92).

To our knowledge, this is presently the most comprehensive metabolic model of potato (93), the third most consumed food crop globally. The secondary metabolism reconstruction is also useful across the *Solanaceae* family, which includes staples, such as tomato and pepper, as well as *Nicotiana* species (94). These economically important plants have large amounts of published data on biotic as well as abiotic stress and combinations thereof available, and are close relatives of potato, meaning that they share with it the majority of their metabolism, including secondary metabolism (40, 41, 95, 96). Therefore, repurposing potato-GEM to study related organisms requires merely i) adapting the secondary metabolism, ii) reconfiguring the biomass function and iii) redefining gene-protein-reaction associations, by finding orthologs from potato or *Arabidopsis* or obtaining them from online databases. Besides repurposing potato-GEM across related species, there are potentially multiple further avenues of future development with this model, such as multitissue (33, 97) and multispecies (98, 99) modeling. Moreover, as a further option to increase the capacity of interpreting growth–defense trade-offs, the metabolic model could be integrated with signaling and regulatory networks, within larger multidomain modeling frameworks (91, 92). Apart from cell maintenance and growth, this would enable capturing also the decision-making activities of the cell, such as sensing and responding to environmental changes and regulating metabolism through the activities and abundances of enzymes (16, 100), likely resulting in a more complete and accurate picture of molecular responses and trade-offs. In regard to agriculture and biotechnology, the model has potential broad applications for crop breeding and metabolic engineering (101, 102). Here, more advanced and complete models enable a larger potential for design of intervention strategies. For instance, as demonstrated by the present analysis of growth–defense and resource trade-offs, the model could be used to optimize resource allocation to develop stress-resistant crop varieties. The underlying aim would be to identify and program plants to simultaneously grow and defend (9, 10), optimizing both functions in terms of specificity and resource consumption, by i) producing only the required defense compounds under certain conditions, ii) optimizing growth by preventing certain resources required for growth to be reallocated to defense, iii) optimizing defense production by identifying and diverting different resources will less impact on growth that could be used for production of the important defense compounds, iv) identifying external conditions or nutrient/resource perturbations that would positively impact growth or defense or their trade-offs, toward stress resistance. Therefore, potato-GEM represents a highly useful resource to study and broaden our understanding of potato as well as general plant defense responses under different types of biotic and abiotic stress.

3. Methods

Metabolic model construction, leaf biomass composition, constraint-based modeling procedures, experimental procedures, transcriptomics data analysis, revision of gene-protein-reaction associations, statistical data analysis, and software usage are detailed in the supplement (*SI Appendix, Supplementary Methods* M1–M8). The model and related files, including Supp. files S1–S6, as well as source code and data to reproduce the results were deposited to the Github repository at https://github.com/NIB-SI/Potato-GEM.

Data, Materials, and Software Availability. Metabolic model and annotations and transcriptomics data have been deposited in GitHub (https://github.com/NIB-SI/Potato-GEM). All other data are included in the article and/or *SI Appendix*.

ACKNOWLEDGMENTS. We thank Phillip Wendering and Anže Županič for technical discussions and critical comments, as well as Živa Ramšak for technical support. The study was supported by the Slovenian Research and Innovation Agency grants no. J2-3060 (J.Z.), Z4-50146 (C.B.) and P4-0165 (K.G.), the Public Scholarship, Development, Disability and Maintenance Fund of the Republic of Slovenia grant no. 11013-9/2021-2 (J.Z.), the European Union Horizon 2020 Framework Programme under grant agreement no. 862858 (https://adapt.univie.ac.at/, K.G.). The European Union's Horizon 2020 research and innovation program also financially supported this work through grant 862201 (to Z.N.). Z.N and S.C. acknowledge the financial support of the Deutsche Forschungsgemeinschaft (DFG, German Research Foundation) - SFB1644/1 - 512328399.

Author affiliations: [a]Department of Biotechnology and Systems Biology, National Institute of Biology, Ljubljana SI1000, Slovenia; [b]Bioinformatics Department, Institute of Biochemistry and Biology, University of Potsdam, Potsdam DE14476, Germany; [c]Systems Biology and Mathematical Modeling, Cooperative Research Group, Max Planck Institute of Molecular Plant Physiology, Potsdam DE14476, Germany; and [d]Department Biologie, Lehrstuhl für Biochemie, Friedrich-Alexander-Universität Erlangen-Nürnberg, Erlangen DE91058, Germany

1. L. T. Hickey *et al.*, Breeding crops to feed 10 billion. *Nat. Biotechnol.* **37**, 744–754 (2019).
2. D. Murphy, *Plants, Biotechnology and Agriculture* (CABI, 2011).
3. S. Savary *et al.*, The global burden of pathogens and pests on major food crops. *Nat. Ecol. Evol.* **3**, 430–439 (2019).
4. A. Maharijaya, B. Vosman, Managing the Colorado potato beetle; The need for resistance breeding. *Euphytica* **204**, 487–501 (2015).
5. N. M. Petrov, M. I. Stoyanova, R. K. Gaur, "Biodiversity and characterization of economically important viruses on potato cultivars" in *Plant RNA Viruses*, R. K. Gaur, B. L. Patil, R. Selvarajan, Eds. (Elsevier, 2023), pp. 245–270.
6. Š. Baebler, A. Coll, K. Gruden, Plant molecular responses to Potato virus Y: A continuum of outcomes from sensitivity and tolerance to resistance. *Viruses* **12**, 217 (2020).
7. S. H. Chung, C. Rosa, K. Hoover, D. S. Luthe, G. W. Felton, Colorado potato beetle manipulates plant defenses in local and systemic leaves. *Plant Signal. Behav.* **8**, e27592 (2013).
8. M. Petek *et al.*, Potato virus Y infection hinders potato defence response and renders plants more vulnerable to Colorado potato beetle attack. *Mol. Ecol.* **23**, 5378–5391 (2014).
9. B. Huot, J. Yao, B. L. Montgomery, S. Y. He, Growth-defense tradeoffs in plants: A balancing act to optimize fitness. *Mol. Plant* **7**, 1267–1287 (2014).
10. Z. He, S. S. Webster, S. He, Growth–defense trade-offs in plants. *Curr. Biol.* **32**, R634–R639 (2022).
11. D. A. Herms, W. J. Mattson, The dilemma of plants: To grow or defend. *Q. Rev. Biol.* **67**, 283–335 (1992).
12. M. Gao, Z. Hao, Y. Ning, Z. He, Revisiting growth-defence trade-offs and breeding strategies in crops. *Plant Biotechnol. J.* **22**, 1198–1205 (2024).
13. K. Yıldırım *et al.*, Genome editing for healthy crops: Traits, tools and impacts. *Front. Plant Sci.* **14**, 1231013 (2023).
14. S. I. Zandalinas *et al.*, Systemic signaling during abiotic stress combination in plants. *Proc. Natl. Acad. Sci. U.S.A.* **117**, 13810–13820 (2020).
15. C. Bleker *et al.*, Stress Knowledge Map: A knowledge graph resource for systems biology analysis of plant stress responses. *Plant Commun.* **5**, 100920 (2024).
16. F. Delplace, C. Huard-Chauveau, R. Berthomé, D. Roby, Network organization of the plant immune system: From pathogen perception to robust defense induction. *Plant J.* **109**, 447–470 (2022).
17. Š. Baebler *et al.*, Dynamics of responses in compatible potato–Potato virus Y interaction are modulated by salicylic acid. *PLoS One* **6**, e29009 (2011).
18. T. Lukan *et al.*, Precision transcriptomics of viral foci reveals the spatial regulation of immune-signaling genes and identifies RBOHD as an important player in the incompatible interaction between potato virus Y and potato. *Plant J.* **104**, 645–661 (2020).
19. N. Töpfer, Environment-coupled models of leaf metabolism. *Biochem. Soc. Trans.* **49**, 119–129 (2021).
20. J. Nielsen, Systems biology of metabolism. *Annu. Rev. Biochem.* **86**, 245–275 (2017).
21. C. M. Rojas, M. Senthil-Kumar, V. Tzin, K. S. Mysore, Regulation of primary plant metabolism during plant-pathogen interactions and its contribution to plant defense. *Front. Plant Sci.* **5**, 17 (2014).
22. M. Zaynab *et al.*, Role of secondary metabolites in plant defense against pathogens. *Microb. Pathog.* **124**, 198–202 (2018).
23. S. Panda, Y. Kazachkova, A. Aharoni, Catch-22 in specialized metabolism: Balancing defense and growth. *J. Exp. Bot.* **72**, 6027–6041 (2021).
24. S. C. Córdoba *et al.*, Identification of gene function based on models capturing natural variability of Arabidopsis thaliana lipid metabolism. *Nat. Commun.* **14**, 4897 (2023).
25. S. Watts, S. Kaur, R. Kariyat, Revisiting plant defense-fitness trade-off hypotheses using *Solanum* as a model genus. *Front. Ecol. Evol.* **10**, 1094961 (2023).

26. E. Shen, T. Zhao, Q.-H. Zhu, Are miRNAs applicable for balancing crop growth and defense trade-off? *New Phytol.* **243**, 1670–1680 (2024).
27. R. Ray *et al.*, A persistent major mutation in canonical jasmonate signaling is embedded in an herbivory-elicited gene network. *Proc. Natl. Acad. Sci. U.S.A.* **120**, e2308500120 (2023).
28. I. Lange, B. M. Lange, D. A. Navarre, Altering potato isoprenoid metabolism increases biomass and induces early flowering. *J. Exp. Bot.* **71**, 4109–4124 (2020).
29. C. Wasternack, I. Feussner, The oxylipin pathways: Biochemistry and function. *Annu. Rev. Plant Biol.* **69**, 363–386 (2018).
30. T. V. Savchenko, O. M. Zastrijnaja, V. V. Klimov, Oxylipins and plant abiotic stress resistance. *Biochemistry (Mosc.)* **79**, 362–375 (2014).
31. I. T. Major *et al.*, Regulation of growth–defense balance by the jasmonate zim-domain (JAZ)-MYC transcriptional module. *New Phytol.* **215**, 1533–1547 (2017).
32. A. Arnold, Z. Nikoloski, Bottom-up metabolic reconstruction of Arabidopsis and its application to determining the metabolic costs of enzyme production. *Plant Physiol.* **165**, 1380–1391 (2014).
33. L. Gerlin, L. Cottret, A. Escourrou, S. Genin, C. Baroukh, A multi-organ metabolic model of tomato predicts plant responses to nutritional and genetic perturbations. *Plant Physiol.* **188**, 1709–1723 (2022).
34. S. Hashemi, R. Laitinen, Z. Nikoloski, Models and molecular mechanisms for trade-offs in the context of metabolism. *Mol. Ecol.* **33**, e16879 (2024).
35. M. Lakshmanan *et al.*, Elucidating rice cell metabolism under flooding and drought stresses using flux-based modeling and analysis. *Plant Physiol.* **162**, 2140–2150 (2013).
36. S. Mintz-Oron *et al.*, Reconstruction of Arabidopsis metabolic network models accounting for subcellular compartmentalization and tissue-specificity. *Proc. Natl. Acad. Sci. U.S.A.* **109**, 339–344 (2012).
37. S. Hashemi, Z. Razaghi-Moghadam, R. A. E. Laitinen, Z. Nikoloski, Relative flux trade-offs and optimization of metabolic network functionalities. *Comput. Struct. Biotechnol. J.* **20**, 3963–3971 (2022).
38. S. Hashemi, Z. Razaghi-Moghadam, Z. Nikoloski, Identification of flux trade-offs in metabolic networks. *Sci. Rep.* **11**, 23776 (2021).
39. S. Colombié *et al.*, Comparative constraint-based modelling of fruit development across species highlights nitrogen metabolism in the growth–defence trade-off. *Plant J.* **116**, 786–803 (2023).
40. Tomato Genome Consortium, The tomato genome sequence provides insights into fleshy fruit evolution. *Nature* **485**, 635–641 (2012).
41. C. Hawkins *et al.*, Plant Metabolic Network 15: A resource of genome-wide metabolism databases for 126 plants and algae. *J. Integr. Plant Biol.* **63**, 1888–1905 (2021).
42. R. Caspi *et al.*, The MetaCyc database of metabolic pathways and enzymes–A 2019 update. *Nucleic Acids Res.* **48**, D445–D453 (2020).
43. P. D. Karp *et al.*, Pathway tools version 23.0 update: Software for pathway/genome informatics and systems biology. *Brief. Bioinform.* **22**, 109–126 (2021).
44. S. H. J. Chan, J. Cai, L. Wang, M. N. Simons-Senftle, C. D. Maranas, Standardizing biomass reactions and ensuring complete mass balance in genome-scale metabolic models. *Bioinformatics* **33**, 3603–3609 (2017).
45. N. Schauer, D. Zamir, A. R. Fernie, Metabolic profiling of leaves and fruit of wild species tomato: A survey of the *Solanum lycopersicum* complex. *J. Exp. Bot.* **56**, 297–307 (2005).
46. A. Pęksa, J. Miedzianka, A. Nemś, E. Rytel, The free-amino-acid content in six potatoes cultivars through storage. *Molecules* **26**, 1322 (2021).
47. B. R. Hastilestari *et al.*, Deciphering source and sink responses of potato plants (Solanum tuberosum L.) to elevated temperatures. *Plant Cell Environ.* **41**, 2600–2616 (2018).
48. S. Santacruz, K. Koch, R. Andersson, P. Aman, Characterization of potato leaf starch. *J. Agric. Food Chem.* **52**, 1985–1989 (2004).
49. L. Chea, A. Meijide, C. Meinen, E. Pawelzik, M. Naumann, Cultivar-dependent responses in plant growth, leaf physiology, phosphorus use efficiency, and tuber quality of potatoes under limited phosphorus availability conditions. *Front. Plant Sci.* **12**, 723862 (2021).
50. K. Mengel, E. A. Kirkby, *Principles of Plant Nutrition* (Springer Science & Business Media, 2012).
51. M. Zagorščak *et al.*, Integration of multi-omics data and deep phenotyping provides insights into responses to single and combined abiotic stress in potato. *Plant Physiol.* **197**, kiaf126 (2025).
52. T. Isah, Stress and defense responses in plant secondary metabolites production. *Biol. Res.* **52**, 39 (2019).
53. A. P. Burgard, E. V. Nikolaev, C. H. Schilling, C. D. Maranas, Flux coupling analysis of genome-scale metabolic network reconstructions. *Genome Res.* **14**, 301–312 (2004).
54. S. Gudmundsson, I. Thiele, Computationally efficient flux variability analysis. *BMC Bioinformatics* **11**, 489 (2010).
55. M. Sajitz-Hermstein, Z. Nikoloski, Multi-objective shadow prices point at principles of metabolic regulation. *Biosystems* **146**, 91–101 (2016).
56. A. G. Pereira *et al.*, "Plant alkaloids: Production, extraction, and potential therapeutic properties" in *Natural Secondary Metabolites: From Nature, through Science, to Industry*, M. Carocho, S. A. Heleno, L. Barros, Eds. (Springer International Publishing, Cham, 2023), pp. 157–200.
57. D. E. Vance, *Biochemistry of Lipids, Lipoproteins and Membranes* (Elsevier Science & Technology, 2008).
58. R. K. Monson, A. M. Trowbridge, R. L. Lindroth, M. T. Lerdau, Coordinated resource allocation to plant growth-defense tradeoffs. *New Phytol.* **233**, 1051–1066 (2022).
59. R. Schwacke *et al.*, MapMan4: A refined protein classification and annotation framework applicable to multi-omics data analysis. *Mol. Plant* **12**, 879–892 (2019).
60. Ž Ramsak *et al.*, GoMapMan: Integration, consolidation and visualization of plant gene annotations within the MapMan ontology. *Nucleic Acids Res.* **42**, D1167–D1175 (2014).
61. A. Subramanian *et al.*, Gene set enrichment analysis: A knowledge-based approach for interpreting genome-wide expression profiles. *Proc. Natl. Acad. Sci. U.S.A.* **102**, 15545–15550 (2005).
62. C. M. J. Pieterse, D. Van der Does, C. Zamioudis, A. Leon-Reyes, S. C. M. Van Wees, Hormonal modulation of plant immunity. *Annu. Rev. Cell Dev. Biol.* **28**, 489–521 (2012).
63. S. E. Milner *et al.*, Bioactivities of glycoalkaloids and their aglycones from Solanum species. *J. Agric. Food Chem.* **59**, 3454–3484 (2011).
64. R. A. Dixon *et al.*, The phenylpropanoid pathway and plant defence-a genomics perspective. *Mol. Plant Pathol.* **3**, 371–390 (2002).
65. P. Kogovšek *et al.*, Primary metabolism, phenylpropanoids and antioxidant pathways are regulated in potato as a response to Potato virus Y infection. *PLoS One* **11**, e0146135 (2016).
66. D. A. T. Boncan *et al.*, Terpenes and terpenoids in plants: Interactions with environment and insects. *Int. J. Mol. Sci.* **21**, 7382 (2020).
67. Z. Iqbal, M. S. Iqbal, A. Hashem, E. F. Abd Allah, M. I. Ansari, Plant defense responses to biotic stress and its interplay with fluctuating dark/light conditions. *Front. Plant Sci.* **12**, 631810 (2021).
68. M. Van Bel *et al.*, PLAZA 5.0: Extending the scope and power of comparative and functional genomics in plants. *Nucleic Acids Res.* **50**, D1468–D1474 (2022).
69. S. F. Altschul, W. Gish, W. Miller, E. W. Myers, D. J. Lipman, Basic local alignment search tool. *J. Mol. Biol.* **215**, 403–410 (1990).
70. G. Moreno-Hagelsieb, K. Latimer, Choosing BLAST options for better detection of orthologs as reciprocal best hits. *Bioinformatics* **24**, 319–324 (2008).
71. I. Thiele, B. Ø. Palsson, A protocol for generating a high-quality genome-scale metabolic reconstruction. *Nat. Protoc.* **5**, 93–121 (2010).
72. K. Hegde, C. M. Kalleshwaraswamy, V. Venkataravanappa, Role of virus infection in seed tubers, secondary spread and insecticidal spray on the yield of potato in Deccan plateau. *Potato Res.* **64**, 339–351 (2021).
73. J. E. Dripps, Z. Smilowitz, Growth analysis of potato plants damaged by Colorado Potato Beetle (Coleoptera: Chrysomelidae) at different plant growth stages. *Environ. Entomol.* **18**, 854–867 (1989).
74. D. E. Kaufman, R. L. Smith, Direction choice for accelerated convergence in hit-and-run sampling. *Oper. Res.* **46**, 84–95 (1998).
75. M. Seyis, Z. Razaghi-Moghadam, Z. Nikoloski, Flux-sum coupling analysis of metabolic network models. *PLoS Comput. Biol.* **21**, e1012972 (2025).
76. B. K. S. Chung, D.-Y. Lee, Flux-sum analysis: A metabolite-centric approach for understanding the metabolic network. *BMC Syst. Biol.* **3**, 117 (2009).
77. S. Robaina-Estévez, D. M. Daloso, Y. Zhang, A. R. Fernie, Z. Nikoloski, Resolving the central metabolism of Arabidopsis guard cells. *Sci. Rep.* **7**, 8307 (2017).
78. D. K. Großkinsky, K. Edelsbrunner, H. Pfeifhofer, E. Graaff, T. Roitsch, Cis- and trans-zeatin differentially modulate plant immunity. *Plant Signal. Behav.* **8**, e24798 (2013).
79. M. Lacuesta *et al.*, The trans and cis zeatin isomers play different roles in regulating growth inhibition induced by high nitrate concentrations in maize. *Plant Growth Regul.* **85**, 199–209 (2018).
80. E. Sharma, G. Anand, R. Kapoor, Terpenoids in plant and arbuscular mycorrhiza-reinforced defence against herbivorous insects. *Ann. Bot.* **119**, 791–801 (2017).
81. P. D. Karp, D. Weaver, M. Latendresse, How accurate is automated gap filling of metabolic models? *BMC Syst. Biol.* **12**, 73 (2018).
82. X. Rao, J. Barros, Modeling lignin biosynthesis: A pathway to renewable chemicals. *Trends Plant Sci.* **29**, 546–559 (2024).
83. J. D. Orth, I. Thiele, B. Ø. Palsson, What is flux balance analysis? *Nat. Biotechnol.* **28**, 245–248 (2010).
84. S. Fallahi, H. J. Skaug, G. Alendal, A comparison of monte carlo sampling methods for metabolic network models. *PLoS One* **15**, e0235393 (2020).
85. D. Cipollini, D. Walters, C. Voelckel, "Costs of resistance in plants: From theory to evidence" in *Annual Plant Reviews Online*, C. Voelckel, G. Jander, Eds. (Wiley, 2017), pp. 263–307.
86. P. D. Coley, J. P. Bryant, F. S. Chapin III, Resource availability and plant antiherbivore defense. *Science* **230**, 895–899 (1985).
87. J. L. Reed, Shrinking the metabolic solution space using experimental datasets. *PLoS Comput. Biol.* **8**, e1002662 (2012).
88. D. Machado, M. Herrgård, Systematic evaluation of methods for integration of transcriptomic data into constraint-based models of metabolism. *PLoS Comput. Biol.* **10**, e1003580 (2014).
89. P. Wendering, G. M. Andreou, R. A. E. Laitinen, Z. Nikoloski, Metabolic modeling identifies determinants of thermal growth responses in *Arabidopsis thaliana*. *New Phytol.* **247**, 178–190 (2025), 10.1111/nph.20420.
90. N. Anjali *et al.*, Role of plant secondary metabolites in defence and transcriptional regulation in response to biotic stress. *Plant Stress* **8**, 100154 (2023).
91. L. Österberg *et al.*, A novel yeast hybrid modeling framework integrating Boolean and enzyme-constrained networks enables exploration of the interplay between signaling and metabolism. *PLoS Comput. Biol.* **17**, e1008891 (2021).
92. B. Schnitzer, L. Österberg, I. Skopa, M. Cvijovic, Multi-scale model suggests the trade-off between protein and ATP demand as a driver of metabolic changes during yeast replicative ageing. *PLoS Comput. Biol.* **18**, e1010261 (2022).
93. K. Botero, S. Restrepo, A. Pinzón, A genome-scale metabolic model of potato late blight suggests a photosynthesis suppression mechanism. *BMC Genomics* **19**, 863 (2018).
94. L. Eidenberger, B. Kogelmann, H. Steinkellner, Plant-based biopharmaceutical engineering. *Nat. Rev. Bioeng.* **1**, 426–439 (2023).
95. K.-I. Kurotani *et al.*, Genome sequence and analysis of *Nicotiana benthamiana*, the model plant for interactions between organisms. *Plant Cell Physiol.* **64**, 248–257 (2023).
96. C. Qin *et al.*, Whole-genome sequencing of cultivated and wild peppers provides insights into *Capsicum* domestication and specialization. *Proc. Natl. Acad. Sci. U.S.A.* **111**, 5135–5140 (2014).
97. R. Shaw, C. Y. M. Cheung, A dynamic multi-tissue flux balance model captures carbon and nitrogen metabolism and optimal resource partitioning during Arabidopsis growth. *Front. Plant Sci.* **9**, 884 (2018).
98. M. Schäfer *et al.*, Metabolic interaction models recapitulate leaf microbiota ecology. *Science* **381**, eadf5121 (2023).
99. V. Mataigne, N. Vannier, P. Vandenkoornhuyse, S. Hacquard, Multi-genome metabolic modeling predicts functional inter-dependencies in the Arabidopsis root microbiome. *Microbiome* **10**, 217 (2022).
100. D. R. Hyduke, B. Ø. Palsson, Towards genome-scale signalling network reconstructions. *Nat. Rev. Genet.* **11**, 297–307 (2010).
101. A. Küken, Z. Nikoloski, Computational approaches to design and test plant synthetic metabolic pathways. *Plant Physiol.* **179**, 894–906 (2019).
102. A. S. Birchfield, C. A. McIntosh, Metabolic engineering and synthetic biology of plant natural products–A minireview. *Curr. Plant Biol.* **24**, 100163 (2020).